



# Large-Area, Free-Standing, Two-Dimensional Supramolecular Polymer Single-Layer Sheets for Highly Efficient Electrocatalytic Hydrogen Evolution

Renhao Dong, Martin Pfeiffermann, Haiwei Liang, Zhikun Zheng, Xiang Zhu, Jian Zhang, and Xinliang Feng\*

**Abstract:** The rational construction of covalent or noncovalent organic two-dimensional nanosheets is a fascinating target because of their promising applications in electronics, membrane technology, catalysis, sensing, and energy technologies. Herein, a large-area (square millimeters) and free-standing 2D supramolecular polymer (2DSP) single-layer sheet (0.7–0.9 nm in thickness), comprising triphenylene-fused nickel bis(dithiolene) complexes has been readily prepared by using the Langmuir–Blodgett method. Such 2DSPs exhibit excellent electrocatalytic activities for hydrogen generation from water with a Tafel slope of 80.5 mV decade<sup>-1</sup> and an overpotential of 333 mV at 10 mA cm<sup>-2</sup>, which are superior to that of recently reported carbon nanotube supported molecular catalysts and heteroatom-doped graphene catalysts. This work is promising for the development of novel free-standing organic 2D materials for energy technologies.

The discovery of graphene has triggered great interest in the design and synthesis of two-dimensional covalent or non-covalent organic nanosheets because of their exceptional physical properties and promising applications in electronics, membrane technology, catalysis, sensing, energy storage, and conversion.<sup>[1–4]</sup> At present, one of the key challenges faced by the research community is the rational construction of free-standing single-atom/monomer-thick organic 2D nanosheets on a large scale. Numerous “top-down” exfoliation strategies have been implemented using carbon nitride,<sup>[5]</sup> layer-structured covalent organic frameworks (COFs),<sup>[6]</sup> and metal-organic frameworks (MOFs)<sup>[7]</sup> to produce free-standing organic 2D nanosheets. One recent intriguing advance is the exfoliation of layered covalent polymer crystals developed by both Schlüter, King, and their respective co-workers,<sup>[3,8]</sup> toward the isolation of 2D polymers (2DPs) composed of single-layer sheets of covalently linked polymers with periodic planar units. Nevertheless, one of the drawbacks of these

“top-down” exfoliation methods is the production of non-uniform nanosheets with varying thicknesses (approximately 1 nm to 7 nm) and limited sizes (200 nm to 30 μm in length). On the other hand, by using the “bottom-up” approach, a variety of structurally precise nanometer-sized π-conjugated graphene fragments and nanoribbons have been chemically synthesized in solution and on solid surfaces,<sup>[9]</sup> but the synthesis of larger graphene-like covalent organic nanosheets remains an enormous challenge.<sup>[10,11]</sup>

Two-dimensional supramolecular polymers (2DSPs),<sup>[4]</sup> which refer to noncovalently linked networks of monomers with periodic bonds along two orthogonal directions, have provided another “bottom-up” route toward the construction of organic 2D nanosheets.<sup>[12–15]</sup> For instance, Nishihara and co-workers<sup>[13]</sup> reported that planar metal bis(dithiolene) complexes can produce highly conductive π-conjugated 2D nanosheets at liquid/liquid and air/water interfaces. One shortcoming of these self-assembly strategies is that they only produce nanosheets with a small lateral dimension (<5 μm).<sup>[14]</sup> Therefore, it is highly appealing to develop a reliable protocol for producing free-standing single-layer sheets with large lateral dimensions (mm<sup>2</sup> or cm<sup>2</sup>) for advanced device applications. To this end, the Langmuir–Blodgett (LB) method represents a promising pathway to create large-area, ordered, thin nanosheets on liquid surfaces. One prominent example is the synthesis of metal-coordinated terpyridine-fused 2DSPs at an air/water interface, with the lateral dimensions reaching several square millimeters.<sup>[15]</sup>

Herein we report the use of the LB method for the fabrication of a novel 2DSP single-layer sheet consisting of nickel bis(dithiolene) complexes at the air/water interface. In our design, 1,2,5,6,9,10-triphenylenehexathiols (THT), a larger π-conjugated monomer, was employed as the key building block (see the Supporting Information for synthetic details and also Figures S1–S3). The lateral dimensions of the fabricated THTNi 2DSP sheet were on the order of square millimeters, and the sheet was 0.7–0.9 nm in thickness; furthermore, the sheet exhibited typical features of free-standing structures. Such 2DSPs can be completely transferred to arbitrary substrates; for instance, the sheets can homogeneously cover glassy carbon electrodes (ca. 20 mm<sup>2</sup>) for electrochemical studies. Remarkably, THTNi 2DSP sheets allow for the sufficient exposure of well-distributed nickel bis(dithiolene) moieties,<sup>[16]</sup> leading to a highly efficient electrocatalytic hydrogen evolution reaction (HER) with a Tafel slope of 80.5 mV decade<sup>-1</sup>, an onset overpotential of 110 mV, and an operating overpotential of 333 mV at

[\*] Dr. R. Dong, Dr. Z. Zheng, Dr. X. Zhu, Dr. J. Zhang, Prof. Dr. X. Feng  
Department of Chemistry and Food Chemistry, and  
Center for Advancing Electronics Dresden  
Technische Universität Dresden  
01062 Dresden (Germany)  
E-mail: xinliang.feng@tu-dresden.de

M. Pfeiffermann, Dr. H. Liang  
Max Planck Institute for Polymer Research  
Ackermannweg 10, 55128 Mainz (Germany)

Supporting information for this article is available on the WWW under <http://dx.doi.org/10.1002/anie.201506048>.



**Figure 1.** Synthesis of a 2DSP single-layer sheet composed of triphenylene-fused nickel bis(dithiolene) complexes by using the Langmuir–Blodgett method at an air/water interface.

$10 \text{ mA cm}^{-2}$ , which are superior to those of recently reported carbon nanotube (CNT)-supported molecular catalysts<sup>[17]</sup> and heteroatom-doped graphene catalysts.<sup>[18]</sup> Therefore, our work provides an appealing strategy for the rational construction of large-area, free-standing 2DSP nanosheets for energy applications.

Figure 1 shows the typical fabrication process of large-area THTNi 2DSP sheets by using the LB method at an air/water interface. A submonolayer of THT monomers was spread over the water surface in an LB trough. After the close packing of the monomers into a dense film upon compression to  $10 \text{ mN m}^{-1}$  (Figure S4), a solution of nickel salts was injected into the water phase. With the diffusion of nickel ions from the bulk phase to the interface, 2D supramolecular polymerization was triggered by the coordination of nickel ions with dithiolene units, resulting in targeted 2DSPs with a large area.

After the vertical transfer of the resulting THTNi 2DSP sheets onto  $300 \text{ nm SiO}_2/\text{Si}$  wafers, optical microscopy (OM), scanning electron microscopy (SEM), and atomic force microscopy (AFM) were used to study the morphology of the THTNi 2DSP sheets. The OM image shows a homogeneous film with long (mm) and straight edges co-occurring with flexible, partially folded sheets (Figure 2a). The straight edges resulted from the rupture of the 2DSP sheet along cleavage lines. The clear contrast between the film (1) and  $\text{SiO}_2$  substrate (0) indicates the ultrathin nature of the THTNi 2DSP sheet. The OM images in Figure S5 show a partial sheet with an area greater than around  $1 \text{ mm}^2$ . SEM imaging (Figure 2c) reveals the absence of layer stacking after vertical transfer. A tapping-mode AFM height image (Figure 2e) and the cross-sectional analysis (Figure S6) indicate that the sheet has a thickness of approximately  $0.7 \text{ nm}$  on  $\text{SiO}_2/\text{Si}$  wafer while its thickness is measured to be about  $0.9 \text{ nm}$  on mica (Figure S7), thus suggesting the single-layer feature of a THTNi 2DSP sheet prepared by the LB method.<sup>[19,20]</sup> Notably, the multilayer structures with controllable numbers of layers could be readily deposited on substrates by a repeated LB transfer process. Figure 2b,d shows bare

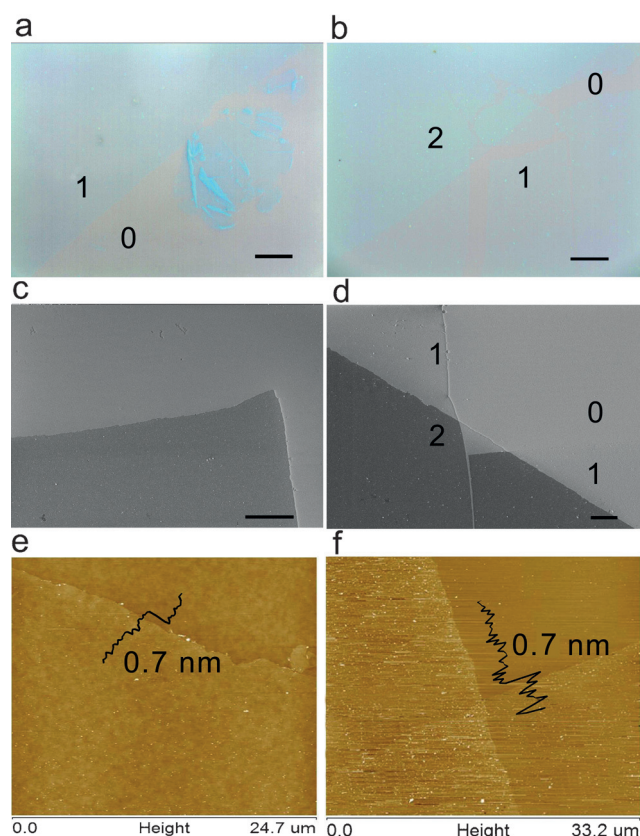


**Figure 2.** Morphology characterization of THTNi 2DSP sheets after vertical transfer onto  $300 \text{ nm SiO}_2/\text{Si}$  wafers. a, b) Optical microscopy images showing large-area 2DSP sheets. Scale bar:  $100 \mu\text{m}$ . c, d) SEM images showing single-layer sheet and multilayer patterns, respectively. Scale bar:  $10 \mu\text{m}$ . The numbers of layers are shown in the image. e, f) Tapping-mode AFM height images and the corresponding cross-sectional analysis demonstrating a single-layer sheet measuring approximately  $0.9 \text{ nm}$  in thickness. The multilayer patterns were prepared by performing repeated transfer steps (b, d, and f).

substrates (0) that contrast with the single-layer (1) and two-layer (2) sheets. The strong reflection contrast between the bare  $\text{SiO}_2$  and organic sheets and the clear film edges helps to identify the number of layers (enlarged versions of the images in Figure 2b,d are shown in Figure S8). AFM height images further indicate that the height difference between each layer was approximately  $0.7 \text{ nm}$  after consecutive LB deposition cycles (Figure 2f).

Next, we horizontally transferred the THTNi 2DSP single-layer sheets onto Cu grids to investigate the morphology, mechanical stability, and internal structure by OM, transmission electron microscopy (TEM), and SEM.<sup>[11,15,19]</sup> Although the sheets tended to shrink to produce a mass of wrinkles during the transfer process, they were stable enough to span over hexagonal holes with an  $18 \mu\text{m}$  side length (Figure 3a,b, Figures S9–11), which is a typical feature of free-standing structures.<sup>[15]</sup> As the single-layer sheets showed low stability under electron irradiation, the selected-area electron diffraction was performed region by region at  $-175^\circ\text{C}$ . Figure S10b shows the typical hexagonal diffraction pattern, thus suggesting the formation of a hexagonal ordered

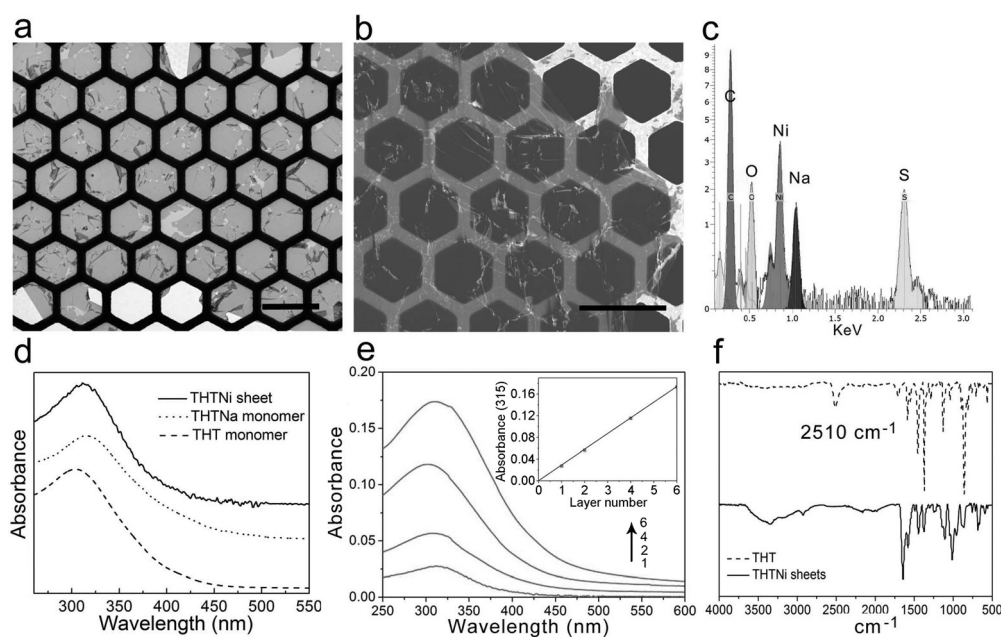


**Figure 3.** Structural characterization of THTNi 2DSP sheets. a, b) TEM and SEM images show the single-layer sheets after horizontal transfer on to Cu grids (hexagonal holes with side length of 18  $\mu\text{m}$ ). c) EDS spectrum revealing the sheet composition with respect to Na, Ni, C, and S. d) UV/Vis spectra of THT monomers (dashed line), THTNa monomers (dotted line), and THTNi 2DSP single-layer sheet (solid line) on quartz wafers. e) UV/Vis spectral change with controlled growth of the thickness from one to six layers on a quartz wafer. Inset: Linear relationship between the absorbance at 315 nm and the layer number. f) FT-IR spectra of a THT monomer (dash line) and THTNi 2DSP multilayer sheets (solid line).

network within the single-layer sheet. Furthermore, the cell length was measured to be 2 nm. We synthesized the bulk THTNi powders under argon, providing indirect proof for the internal structure of single-layer sheets. Powder X-ray diffraction (PXRD) analysis of THTNi bulk materials showed a crystalline structure with a prominent (100) peak and (200) peak at  $2\theta = 4.5^\circ$  and  $9.1^\circ$ , respectively, which is indicative of hexagonal packing within the *ab* planes (Figure S12).<sup>[19]</sup> The peak at  $2\theta = 27.5^\circ$ , corresponding to the (001) reflections, showed the ordered stacking along the *c* direction, as expected for layered materials.<sup>[19]</sup> Calculated from the peak at  $2\theta = 4.5^\circ$ , the pore diameter is about 2 nm, corresponding to the model of molecular nickel bis(dithiolene) units. In conjunction with the TEM and XRD measurements, our results provide strong evidence for the internal hexagonal network structure of the THTNi 2DSP single-layer sheets.

We used energy-dispersed X-ray spectroscopy (EDS) analysis to probe the chemical composition of the sheets (Figure 3c). The presence of Na, Ni, C, and S was detected in the THTNi 2DSP sheets. The oxygen signal may have originated from an adsorbed  $\text{H}_2\text{O}$  layer or the  $\text{SiO}_2/\text{Si}$  substrate. Quantitative analysis of the signals suggests a Ni (4.47 atom %)/S (16.32 atom %) ratio of approximately 1:3.6, which is very close to the composition of nickel bis(dithiolene) linkers (Ni/S = 1:4). This result is strong evidence for the high degree of coordination between Ni ions and thiol groups throughout the 2DSP sheet, in accordance with the results obtained by X-ray photoelectron spectroscopy (XPS; see below).

The UV/Vis spectrum shows a broad band between 300 and 400 nm (Figure 3d) for the THTNi 2DSP single-layer sheet transferred onto a quartz wafer, which is analogous to that observed in the UV/Vis spectra of THT and hexasodiumtriphenylenehexathiolate (THTNa) monomers, thus confirming the presence of triphenylene-fused building blocks in the sheet. To study the changes of the optical properties with the controlled growth of the sheet thickness, the single-layer nanosheets were deposited repeatedly on a quartz wafer at a constant surface pressure by using the horizontal transfer method. Figure 3e shows the UV/Vis spectra of the deposited THTNi 2DSP sheets with different layer numbers and the peak absorbance at

315 nm is proportional to the layer number (Figure 3e inset, and Figure S13), thus indicating quantitative, layer-by-layer accumulation of single-layer nanosheet.<sup>[15c]</sup> The attenuated total reflection IR (ATR-IR) spectra of the THTNi 2DSP few-layer sheets and THT monomer are compared in Figure 3f. Although the THT monomer showed a strong signal at  $2510\text{ cm}^{-1}$  attributable to the S–H stretching vibrations, this peak vanished in the spectrum of the THTNi 2DSP sheet, thus suggesting that the thiol groups were efficiently coordinated to  $\text{Ni}^{2+}$  ions to form nickel bis(dithiolene) linkers.<sup>[12]</sup>

To further probe the chemical composition of the THTNi 2DSP sheets, XPS measurements were conducted on a  $\text{SiO}_2/\text{Si}$  substrate. The spectrum shows the presence of Na 1s, Ni 2s, Ni 2p, C 1s, S 2s, and S 2p core levels (Figure 4a). Relative to the XPS spectrum of the THT monomer (Figure S14), the appearance of a Ni signal in the sheet confirms that the addition of Ni salts induced the polymerization of the monomers. The high-resolution Ni 2p photoemission spectrum shows two sets of peaks (Figure S15), with binding energies of 855 and 872 eV, which correspond to the 2p<sub>3/2</sub> and 2p<sub>1/2</sub> levels, respectively. This result signifies that a single type of Ni atom occurred in the THTNi 2DSP sheet, without the presence of extraneous  $\text{Ni}^{2+}$  ions.<sup>[12,21]</sup> The Na impurity (1.8 at. %) actually originates from the introduction of  $\text{NaNO}_3$ , which was for the ion compensation when the Ni ions were linked to the thiol groups. However, it is difficult to completely remove the Na salts from the layer surface by water and chloroform washing, thus leading to the detection of Na element by EDS (Figure 3c) and XPS (Figure 4a, Figures S16 and S17). The S 2p peak in the XPS spectrum

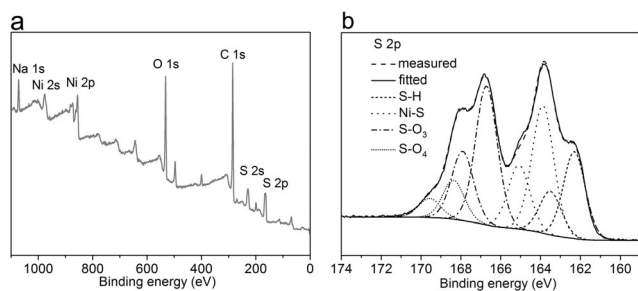


**Figure 4.** XPS analysis of THTNi 2DSP sheets. a) Energy survey spectrum. b) High-resolution spectrum in the S 2p region. The doublet peaks with an intensity ratio of 1:2 result from spin-orbit coupling, with  $\Delta = 1.2$  eV, and are characteristic of the S 2p<sub>3/2</sub> and 2p<sub>1/2</sub> orbitals.

occurs at a binding energy of approximately 165 eV (Figure 4a). Deconvolution of the S 2p signal generates four sets of doublets (Figure 4b). The high-intensity doublets at 163.8 and 165.1 eV are derived from the Ni-S units, and strongly indicate efficient complexation between Ni<sup>2+</sup> ions and thiol groups.<sup>[16]</sup> Quantitative analysis of the Ni and S signals suggests a Ni/S ratio of approximately 1:4.8, for which the sulfur composition is slightly higher than expected (1:4 for the THTNi 2DSP). The oxidation states of sulfur, S-O<sub>3</sub> and S-O<sub>4</sub> are also shown (from 166.7 eV to 169.5 eV). We attribute these states to the partial oxidation of thiol groups when exposed to air during the LB process.<sup>[22]</sup> Furthermore, the weak doublets at 162.3 and 163.5 eV can be ascribed to the partially uncoordinated -SH residues. Based on these peaks, the defect density of the THTNi 2DSP sheet can be calculated as  $35 \pm 10$  atom %. Nevertheless, in conjunction with the XPS, EDS, and IR measurements, our results strongly suggest that the high degree of complexation between Ni<sup>2+</sup> ions and thiol groups was responsible for the formation of large-area, free-standing 2DSP single-layer sheets at the air/water interface.

$\pi$ -conjugated metal bis(dithiolene) moieties are well known to be active sites of molecular catalysis for photocatalytic and electrocatalytic H<sub>2</sub> generation from water.<sup>[16]</sup> Since the stoichiometric evolution of H<sub>2</sub> by reacting iron bis(benzenedithiolate) with HCl was reported,<sup>[23]</sup> a number of transition-metal dithiolate complexes have been developed for the HER.<sup>[16]</sup> These molecular metal dithiolate catalysts are typically employed in aqueous and aqueous/organic media. Thus, it is essential to immobilize these molecular catalysts onto electrode surfaces in a well-defined manner without loss of reactivity and stability.<sup>[17]</sup> Given that the THTNi 2DSP single-layer sheets produced in this study possessed a high density of well-positioned nickel bis(dithiolene) motifs, the sheets could be directly deposited over a large area on an electrode surface, thus functioning as a good candidate for electrochemical water splitting. Hence, the electrocatalytic performance of the THTNi 2DSP sheets in the HER was evaluated by using the rotating disk electrode (RDE) technique in an argon-saturated aqueous solution.

Figure 5a shows the HER polarization curves of a THTNi 2DSP sheet-modified electrode and a bare electrode in a 0.5 M H<sub>2</sub>SO<sub>4</sub> solution. With the THTNi 2DSP sheet catalyst, electrocatalytic hydrogen evolution occurred with an over-

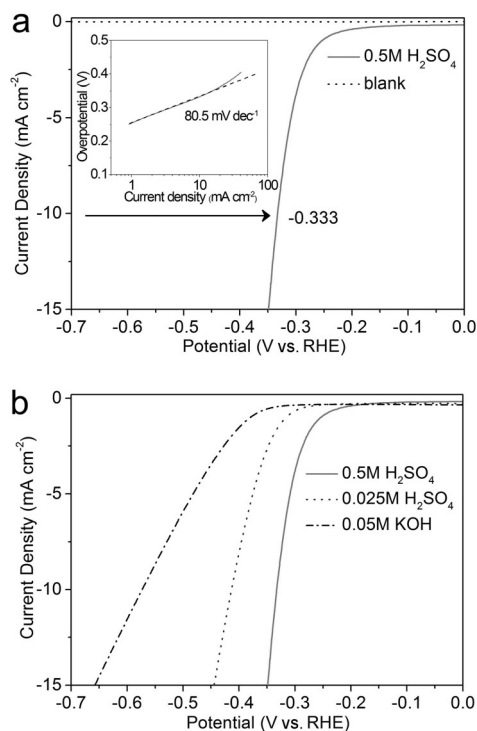


**Figure 5.** Electrocatalytic performance of the THTNi 2DSP sheet and GC electrode. a) HER polarization plots of the THTNi 2DSP sheet and blank glassy carbon disk electrode in 0.5 M H<sub>2</sub>SO<sub>4</sub>. The inset in (a) shows the corresponding Tafel plot. The Tafel slope is 80.5 mVdecade<sup>-1</sup>. b) HER polarization plots in different electrolyte solutions: 0.5 M H<sub>2</sub>SO<sub>4</sub> (pink line), 0.025 M H<sub>2</sub>SO<sub>4</sub> (blue line), and 0.05 M KOH (black line). Electrode rotation speed 1600 rpm; scan rate 10 mV<sup>-1</sup>.

potential of approximately 110 mV, above which the current density increased rapidly. The operating potential at 10 mA cm<sup>-2</sup> was determined to be 333 mV. The inset in Figure 5a shows the Tafel plot of the polarization curve, which provides some insight into the HER pathways. The Tafel slope is 80.5 mVdecade<sup>-1</sup>, thus suggesting that initial proton adsorption, that is, a Volmer reaction, is the rate-determining step of the HER.<sup>[24]</sup> Based on extrapolation from the Tafel plot, the HER exchange current density (*i*<sub>0</sub>) was calculated to be around  $6 \times 10^{-4}$  mA cm<sup>-2</sup>. These values are clearly superior to those reported for molecular catalysts attached on carbon nanotubes.<sup>[17]</sup> For instance, CNT-supported nickel bis(diphosphine) complexes required a higher onset overpotential of about 290 mV and a higher operating overpotential of 300 mV to achieve a HER current density of 4 mA cm<sup>-2</sup>,<sup>[17a]</sup> whereas the CNT-supported cobalt diimine-dioxime complex afforded an onset overpotential of approximately 350 mV, a Tafel slope of 160 mV decade<sup>-1</sup>, and an operating overpotential of 590 mV at 4 mA cm<sup>-2</sup>.<sup>[17b]</sup> Moreover, the electrocatalytic performance of the THTNi 2DSP sheets is superior to that of recently developed N-, P-, or S-doped graphene materials (onset overpotentials 130–380 mV, Tafel slopes 81–130 mV decade<sup>-1</sup>, *i*<sub>0</sub>  $9 \times 10^{-6}$ – $2 \times 10^{-4}$  mA cm<sup>-2</sup>, and operating potentials 280–550 mV at 10 mA cm<sup>-2</sup>),<sup>[18]</sup> and the performance is even comparable to that of many non-noble metal catalysts (Table S1), including

Co or Ni-embedded nitrogen-rich carbon nanotubes,<sup>[24a]</sup> MoS<sub>2</sub> nanosheets,<sup>[24b,c,d]</sup> and WS<sub>2</sub> nanosheets.<sup>[24e]</sup>

The performance of the THTNi 2DSP sheets in the HER was further investigated in various electrolytes with different pH values. Figure 5b shows that an operating overpotential of 413 mV was required to achieve a current density of 10 mA cm<sup>-2</sup> in 0.025 M H<sub>2</sub>SO<sub>4</sub> (pH 1.3), whereas the operating overpotential was 574 mV at 10 mA cm<sup>-2</sup> in 0.05 M KOH (pH 15.3). These values still exceed those of CNT-supported molecular catalysts<sup>[17]</sup> and N-, P-, or S-doped graphene.<sup>[18]</sup> Therefore, these results suggest that the THTNi 2DSP sheets composed of nickel bis(dithiolene) can function as HER catalysts over a wide pH range. In addition, the existence of a small amount of Na<sup>+</sup> ions has no apparent influence on the HER performance of the THTNi 2DSP layers (Figure S18). Interestingly, during the preparation of our manuscript, Marinescu and co-workers reported the fabrication of a triphenylene-fused cobalt bis(dithiolene) film with approximately 360 nm thickness that required a much higher operating overpotential of 530 mV vs. SHE at 10 mA cm<sup>-2</sup> and pH 1.3.<sup>[19]</sup> The outstanding electrocatalytic performance of THTNi 2DSP sheets can be attributed to their large-area, thin-monolayer feature, which allowed for sufficient exposure of well-positioned electrocatalytic active sites during the electrochemical process.

In conclusion, we have demonstrated the preparation of a novel, large-area (on the order of square millimeters) and free-standing 2DSP single-layer sheet consisting of triphenylene-fused nickel bis(dithiolene) complexes at an air/water interface. The high degree of complexation between Ni and thiol groups plays a key role in the robust coupling of the THT monomers. Significantly, a THTNi 2DSP sheet immobilized on an electrode surface exhibited outstanding electrocatalytic performance in the HER; this performance is superior to that of recently reported CNT-supported molecular catalysts and heteroatom-doped graphene catalysts. This work provides important insights suggesting that rationally designed 2DSPs can serve as novel electrode materials for energy applications.

## Acknowledgements

This work was financially supported by the ERC Grant 2DMATER and the EC under the Graphene Flagship (no. CNECT-ICT-604391). R.H.D. gratefully acknowledges funding from the Alexander von Humboldt Foundation. We acknowledge Dr. Petr Formanek for suggestions on the TEM measurements, and we would like to thank Prof. Paolo Samori and Dr. Yuanzhi Tan for helpful discussions.

**Keywords:** electrocatalysis · hydrogen evolution reaction · nanostructures · polymers · supramolecular chemistry

**How to cite:** *Angew. Chem. Int. Ed.* **2015**, *54*, 12058–12063  
*Angew. Chem.* **2015**, *127*, 12226–12231

[1] K. S. Novoselov, A. K. Geim, S. V. Morozov, D. Jiang, Y. Zhang, S. V. Dubonos, I. V. Grigorieva, A. A. Firsov, *Science* **2004**, *306*, 666.

- [2] J. W. Colson, W. R. Dichtel, *Nat. Chem.* **2013**, *5*, 453.  
 [3] J. Sakamoto, J. Heijst, O. Lukin, A. D. Schlüter, *Angew. Chem. Int. Ed.* **2009**, *48*, 1030; *Angew. Chem.* **2009**, *121*, 1048.  
 [4] X. Zhuang, Y. Mai, D. Wu, F. Zhang, X. Feng, *Adv. Mater.* **2015**, *27*, 403.  
 [5] a) Y. Wang, X. Wang, M. Antonietti, *Angew. Chem. Int. Ed.* **2012**, *51*, 68; *Angew. Chem.* **2012**, *124*, 70; b) X. Zhang, X. Xie, H. Wang, J. Zhang, B. Pan, Y. Xie, *J. Am. Chem. Soc.* **2013**, *135*, 18.  
 [6] a) D. N. Bunck, W. R. Dichtel, *J. Am. Chem. Soc.* **2013**, *135*, 14952; b) I. Berlanga, M. L. Ruiz-González, J. M. González-Calbet, J. L. G. Fierro, R. Mas-Ballesté, F. Zamora, *Small* **2011**, *7*, 1207; c) S. Chandra, S. Kandambeth, B. P. Biswal, B. Lukose, S. M. Kunjir, M. Chaudhary, R. Babarao, T. Heine, R. Banerjee, *J. Am. Chem. Soc.* **2013**, *135*, 17853.  
 [7] a) P. Li, Y. Maedaa, Q. Xu, *Chem. Commun.* **2011**, 47, 8436; b) P. Amo-Ochoa, L. Welte, R. González-Prieto, P. J. S. Miguel, C. J. Gómez-García, E. Mateo-Martí, S. Delgado, J. Gómez-Herrerob, F. Zamora, *Chem. Commun.* **2010**, 46, 3262; c) Y. Peng, Y. Li, Y. Ban, H. Jin, W. Jiao, X. Liu, W. Yang, *Science* **2014**, *346*, 1356.  
 [8] a) P. Kissel, R. Erni, W. B. Schweizer, M. D. Rossell, B. T. King, T. Bauer, S. Götzinger, A. D. Schlüter, J. Sakamoto, *Nat. Chem.* **2012**, *4*, 287; b) R. Bhola, P. Payamyar, D. J. Murray, B. Kumar, A. J. Teator, M. U. Schmidt, S. M. Hammer, A. Saha, J. Sakamoto, A. D. Schlüter, B. T. King, *J. Am. Chem. Soc.* **2013**, *135*, 14134; c) P. Kissel, D. J. Murray, W. J. Wulftange, V. J. Catalano, B. T. King, *Nat. Chem.* **2014**, *6*, 774; d) M. J. Kory, M. Wörle, T. Weber, P. Payamyar, S. W. van de Poll, J. Dshemuchadse, N. Trapp, A. D. Schlüter, *Nat. Chem.* **2014**, *6*, 779.  
 [9] L. Chen, Y. Hernandez, X. Feng, K. Müllen, *Angew. Chem. Int. Ed.* **2012**, *51*, 7640; *Angew. Chem.* **2012**, *124*, 7758.  
 [10] K. Baek, G. Yun, Y. Kim, D. Kim, R. Hota, I. Hwang, D. Xu, Y. H. Ko, G. H. Gu, J. H. Suh, C. G. Park, B. J. Sung, K. Ki, *J. Am. Chem. Soc.* **2013**, *135*, 6523.  
 [11] D. J. Murray, D. D. Patterson, P. Payamyar, R. Bhola, W. Song, M. Lackinger, A. D. Schlüter, B. T. King, *J. Am. Chem. Soc.* **2015**, *137*, 3450.  
 [12] K. Zhang, J. Tian, D. Hanifi, Y. Zhang, A. C. Sue, T. Zhou, L. Zhang, X. Zhao, Y. Liu, Z. Li, *J. Am. Chem. Soc.* **2013**, *135*, 17913.  
 [13] T. Kambe, R. Sakamoto, K. Hoshiko, K. Takada, M. Miyachi, J. Ryu, S. Sasaki, J. Kim, K. Nakazato, M. Takata, H. Nishihara, *J. Am. Chem. Soc.* **2013**, *135*, 2462.  
 [14] a) Y. Zheng, H. Zhou, D. Liu, G. Floudas, M. Wagner, K. Koynov, M. Mezger, H. Butt, T. Ikeda, *Angew. Chem. Int. Ed.* **2013**, *52*, 4845; *Angew. Chem.* **2013**, *125*, 4945; b) E. Lee, J. Kim, M. Lee, *Angew. Chem. Int. Ed.* **2009**, *48*, 3657; *Angew. Chem.* **2009**, *121*, 3711.  
 [15] a) T. Bauer, Z. Zheng, A. Renn, R. Enning, A. Stemmer, J. Sakamoto, A. D. Schlüter, *Angew. Chem. Int. Ed.* **2011**, *50*, 7879; *Angew. Chem.* **2011**, *123*, 8025; b) Z. Zheng, L. Opilik, F. Schiffmann, W. Liu, G. Bergamini, P. Ceroni, L. Lee, A. Schütz, J. Sakamoto, R. Zenobi, J. VandeVondele, A. D. Schlüter, *J. Am. Chem. Soc.* **2014**, *136*, 6103; c) R. Sakamoto, K. Hoshiko, Q. Liu, T. Yagi, T. Nagayama, S. Kusaka, M. Tsuchiya, Y. Kitagawa, W. Wong, H. Nishihara, *Nat. Commun.* **2015**, *6*, 6713.  
 [16] a) W. R. McNamara, Z. Han, C. Yin, W. W. Brennessel, P. L. Holland, R. Eisenberg, *Proc. Natl. Acad. Sci. USA* **2012**, *109*, 15594; b) A. Das, Z. Han, W. W. Brennessel, P. L. Holland, R. Eisenberg, *ACS Catal.* **2015**, *5*, 1397.  
 [17] a) A. Le Goff, V. Artero, B. Jusselme, P. D. Tran, N. Guillet, R. Métayé, A. Fihri, S. Palacin, M. Fontecave, *Science* **2009**, *326*, 1384; b) E. S. Andreiadis, P. Jacques, P. D. Tran, A. Leyris, M. Chavarot-Kerlidou, B. Jusselme, M. Matheron, J. Pécaut, S. Palacin, M. Fontecave, V. Artero, *Nat. Chem.* **2013**, *5*, 48.

- [18] a) Y. Zheng, Y. Jiao, L. H. Li, T. Xing, Y. Chen, M. Jaroniec, S. Z. Qiao, *ACS Nano* **2014**, *8*, 5290; b) Y. Ito, W. Cong, T. Fujita, Z. Tang, M. Chen, *Angew. Chem. Int. Ed.* **2015**, *54*, 2131; *Angew. Chem.* **2015**, *127*, 2159.
- [19] a) A. J. Clough, J. W. Yoo, M. H. Mecklenburg, S. C. Marinescu, *J. Am. Chem. Soc.* **2015**, *137*, 118; b) M. G. Campbell, D. Sheberla, S. F. Liu, T. M. Swager, M. Dincă, *Angew. Chem. Int. Ed.* **2015**, *54*, 4349; *Angew. Chem.* **2015**, *127*, 4423.
- [20] D. Adam, P. Schuhmacher, J. Simmerer, L. Häussling, K. Siemensmeyer, K. H. Etzbach, H. Ringsdorf, D. Haarer, *Nature* **1994**, *371*, 141.
- [21] a) J. Cui, Z. Xu, *Chem. Commun.* **2014**, *50*, 3986; b) D. Sheberla, L. Sun, M. A. Blood-Forsythe, S. Er, C. R. Wade, C. K. Brozek, A. Aspuru-Guzik, M. Dincă, *J. Am. Chem. Soc.* **2014**, *136*, 8859.
- [22] J. Baltrusaitis, D. M. Cwiertnyab, V. H. Grassian, *Phys. Chem. Chem. Phys.* **2007**, *9*, 5542.
- [23] D. Sellmann, M. Geck, M. Moll, *J. Am. Chem. Soc.* **1991**, *113*, 5259.
- [24] a) X. Zou, X. Huang, A. Goswami, R. Silva, B. R. Sathe, E. Mikmekov, T. Asefa, *Angew. Chem. Int. Ed.* **2014**, *53*, 4372; *Angew. Chem.* **2014**, *126*, 4461; b) J. Kibsgaard, Z. Chen, B. N. Reinecke, T. F. Jaramillo, *Nat. Mater.* **2012**, *11*, 963; c) J. Xie, H. Zhang, S. Li, R. Wang, X. Sun, M. Zhou, J. Zhou, X. W. Lou, Y. Xie, *Adv. Mater.* **2013**, *25*, 5807; d) M. A. Lukowski, A. S. Daniel, F. Meng, A. Forticaux, L. Li, S. Jin, *J. Am. Chem. Soc.* **2013**, *135*, 10274; e) D. Voiry, H. Yamaguchi, J. Li, R. Silva, D. C. B. Alves, T. Fujita, M. Chen, T. Asefa, V. B. Shenoy, G. Eda, M. Chhowalla, *Nat. Mater.* **2013**, *12*, 850.

Received: July 1, 2015

Revised: August 7, 2015

Published online: August 26, 2015